frontiers in Veterinary Science

ORIGINAL RESEARCH
published: 16 August 2021
doi: 10.3389/fvets.2021.727155

Right Ventricular Myocardial Adaptation Assessed by Two-Dimensional Speckle Tracking Echocardiography in Canine Models of Chronic Pulmonary Hypertension

Yunosuke Yuchi, Ryohei Suzuki, Haruka Kanno, Takahiro Teshima, Hirotaka Matsumoto and Hidekazu Koyama*

Laboratory of Veterinary Internal Medicine, Faculty of Veterinary Science, School of Veterinary Medicine, Nippon Veterinary and Life Science University, Musashino, Japan

OPEN ACCESS

Edited by:
Zeki Yilmaz,
Faculty of Veterinary Medicine, Turkey

Reviewed by:
Domenico Caivano,
University of Perugia, Italy
Enrica Zucca,
University of Milan, Italy

***Correspondence:**
Ryohei Suzuki
ryoheisuzuki@nvlu.ac.jp

Specialty section:
This article was submitted to Comparative and Clinical Medicine, a section of the journal Frontiers in Veterinary Science

Received: *18 June 2021*
Accepted: *22 July 2021*
Published: *16 August 2021*

Citation:
Yuchi Y, Suzuki R, Kanno H, Teshima T, Matsumoto H and Koyama H (2021) Right Ventricular Myocardial Adaptation Assessed by Two-Dimensional Speckle Tracking Echocardiography in Canine Models of Chronic Pulmonary Hypertension. Front. Vet. Sci. 8:727155. doi: 10.3389/fvets.2021.727155

Background: Pulmonary hypertension (PH) is a life-threatening disease in dogs characterized by an increase in pulmonary arterial pressure (PAP) and/or pulmonary vascular resistance. Right ventricle adapts to its pressure overload through various right ventricular (RV) compensative mechanisms: adaptive and maladaptive remodeling. The former is characterized by concentric hypertrophy and increased compensatory myocardial contractility, whereas the latter is distinguished by eccentric hypertrophy associated with impaired myocardial function.

Objectives: To evaluate the RV adaptation associated with the increase of PAP using two-dimensional speckle tracking echocardiography.

Animals: Seven experimentally induced PH models.

Methods: Dogs were anesthetized and then a pulmonary artery catheter was placed via the right jugular vein. Canine models of PH were induced by the repeated injection of microspheres through the catheter and monitored pulmonary artery pressure. Dogs were performed echocardiography and hemodynamic measurements in a conscious state when baseline and systolic PAP (sPAP) rose to 30, 40, 50 mmHg, and chronic phase. The chronic phase was defined that the sPAP was maintained at 50 mmHg or more for 4 weeks without injection of microspheres.

Results: Pulmonary artery to aortic diameter ratio, RV area, end-diastolic RV wall thickness, and RV myocardial performance index were significantly increased in the chronic phase compared with that in the baseline. Tricuspid annular plane systolic excursion was significantly decreased in the chronic phase compared with that in the baseline. The RV longitudinal strain was significantly decreased in the sPAP30 phase, increased in the sPAP40 and sPAP50 phases, and decreased in the chronic phase.

Conclusions: Changes in two-dimensional speckle tracking echocardiography-derived RV longitudinal strain might reflect the intrinsic RV myocardial contractility during the PH progression, which could not be detected by conventional echocardiographic parameters.

Keywords: dog, right ventricular remodeling, right ventricular strain, right ventricular-arterial coupling, wall stress, myocardial function

INTRODUCTION

Pulmonary hypertension (PH), a life-threatening disease in dogs, is characterized by increased pulmonary arterial pressure (PAP, normal range: systolic PAP; 15–25 mmHg, mean PAP; 10–15 mmHg, and diastolic PAP; 5–10 mmHg) and/or pulmonary vascular resistance (1, 2). The disease would be caused by various diseases in dogs, including pulmonary arterial disease, left heart disease, respiratory disease, hypoxia, pulmonary embolic disease, parasitic disease, or some combination of these (1). Recent studies have reported that PH was one of the risk factors for the worse outcome especially in dogs with myxomatous mitral valve disease and respiratory disease/hypoxia (3, 4). Considering the structural characteristics of the right ventricle, the right ventricular (RV) pressure overload would critically impact RV function and cardiac output (5). In humans, to compensate for low cardiac output due to increased PAP, the right ventricle responds through two compensatory mechanisms: adaptive and maladaptive remodeling (6–9). The former is characterized by concentric hypertrophy and increased compensatory myocardial contractility, whereas the latter is distinguished by eccentric hypertrophy associated with impaired myocardial function. Therefore, to estimate the progression of PH, the change in RV myocardial function and remodeling associated with increasing RV pressure overload must be evaluated.

Currently, various echocardiographic variables are used as clinical, non-invasive tools to assess RV function in veterinary medicine; specifically, two-dimensional speckle tracking echocardiography (2D-STE) enables quantitative, non-invasive assessment of the intrinsic RV myocardial function (10–12). However, studies that have assessed the relationship between invasively measured PAP and echocardiographic variables for RV function in the same individuals are limited (13, 14). Furthermore, almost all these studies have evaluated the association in the acute phase of RV pressure overload in anesthetized dogs (13, 14), although in majority of the cases, PH runs a chronic course and various RV adaptations are exhibited.

We hypothesized that 2D-STE indices would reflect the changes in RV function associated with RV adaptation, and there would be differences in RV function between the acute and chronic phase of RV pressure overload. This study aimed to assess RV morphology and function associated with the increase in PAP during the process of creating model dogs with chronic PH.

Abbreviations: 2D-STE, two-dimensional speckle tracking echocardiography; 3seg, only right ventricular free wall analysis; 6seg, right ventricular global analysis; CV, coefficient of variation; PA:Ao, pulmonary artery to aortic diameter ratio; PAP, pulmonary arterial pressure; PH, pulmonary hypertension; RV CO, right ventricular cardiac output; RV FACn, right ventricular fractional area change normalized by body weight; RV MPI, right ventricular myocardial performance index; RV s', tissue Doppler imaging-derived peak systolic myocardial velocity of lateral tricuspid annulus; RV SV, right ventricular stroke volume; RVEDA index, end-diastolic right ventricular area normalized by body weight; RVESA index, end-systolic right ventricular area normalized by body weight; RV-SL, right ventricular longitudinal strain; RV-SrL, right ventricular longitudinal strain rate; RVWTd, end-diastolic right ventricular wall thickness; TAPSEn, tricuspid annular plane systolic excursion normalized by body weight.

MATERIALS AND METHODS

Our prospective, experimental study consisted of procedures that were performed in accordance with the Guide for Institutional Laboratory Animal Care and Use in Nippon Veterinary and Life Science University and was approved by the ethical committee for laboratory animal use of the Nippon Veterinary and Life Science University, Japan (approval number: 2019S-56).

Animals

Seven laboratory male beagles (body weight: 9.1 ± 1.5 kg, age: 1.0 ± 0.2 years) were used in this study. All dogs were determined to be healthy based on a complete physical examination, blood tests, thoracic and abdominal radiography, transthoracic and abdominal ultrasonography, and oscillometric method-derived blood pressure measurement.

Study Preparation

The study dogs were administered butorphanol tartrate (0.2 mg/kg, IV) (Meiji Seika Pharma Co. Ltd., Tokyo, Japan), midazolam hydrochloride (0.2 mg/kg, IV) (Maruishi Pharmaceutical. Co., Ltd., Osaka, Japan), heparin sodium (100 IU/kg, IV) (AY Pharmaceuticals Co. Ltd., Tokyo, Japan), and cefazolin sodium hydrate (20 mg/kg, IV) (LTL Pharma Co. Ltd., Tokyo, Japan) as pre-anesthetic medication. They were then anesthetized intravenously with propofol (Nichi-Iko Pharmaceutical Co., Ltd., Toyama, Japan), maintained with 1.5–2.0% isoflurane (Mylan Seiyaku Ltd., Osaka, Japan) mixed with 100% oxygen. The end-tidal partial pressure of carbon dioxide was monitored and maintained between 35 and 45 mmHg by manual ventilation at a rate of 8–12 breaths per minute. The anesthetized dogs were placed in left lateral recumbency and the right lateral neck region was clipped, prepared aseptically, and draped. An ∼5.0-cm surgical cutdown was performed over the right jugular furrow to exteriorize the right jugular vein. Then an 8-Fr multipurpose catheter (Atom Medical Corp., Tokyo, Japan) was placed in the main pulmonary artery under fluoroscopic guidance. The right side of the neck was sutured, and all the dogs

completely recovered from anesthesia through the conventional method (15).

Creating Model Dogs With Chronic PH and Hemodynamic Measurements

The PAP was measured using circulatory function analysis software (SBP2000, Softron, Tokyo, Japan). The conscious dogs were restrained in the most stable position, and the PAP (systolic, mean, and diastolic) was measured invasively by calibrating with the atmospheric pressure. The average value of PAP calculated from nine consecutive cardiac cycles was considered as "baseline" data and used for the statistical analysis. After baseline PAP measurements were taken, microspheres measuring between 150 and 300 μm in diameter (Sephadex G-25 Coarse, Cytiva, Tokyo, Japan) were injected repeatedly and the peripheral pulmonary artery was embolized via the prepared catheter (16, 17). The time points at which systolic PAP (sPAP) rose to ∼30, 40, and 50 mmHg were defined as "sPAP30," "sPAP40," and "sPAP50," respectively. Each time point was at least 2 days after injection of the microspheres to eliminate the acute effects of microspheres on RV function. When the sPAP was maintained at 50 mmHg or more for 4 weeks without injection of microspheres, the time point was defined as "chronic" and the same examinations as those carried out at the other time points were performed. At each time point, the systemic arterial pressure was measured for all dogs using the oscillometric method. The dogs were sedated using butorphanol tartrate (0.1 mg/kg, IV) and midazolam hydrochloride (0.1 mg/kg, IV) to perform the microsphere injection, PAP measurements, and echocardiography when necessary.

Echocardiographic Assessment of the Right Heart

Echocardiography was performed in all dogs on the same day as the hemodynamic measurements were taken at all time points. Conventional 2D and Doppler examinations were performed by a single investigator (RS) using a Vivid 7 or Vivid E95 echocardiographic system (GE Healthcare, Tokyo, Japan) and a 3.5–6.9 MHz transducer. A lead II electrocardiogram was recorded simultaneously and the images were displayed. Data obtained from at least five consecutive cardiac cycles in sinus rhythm from the dogs that were manually restrained in right and left lateral recumbency were stored. The images were analyzed using an offline workstation (EchoPAC PC, Version 204; GE Healthcare, Tokyo, Japan) by a single observer (YY).

For studying the right heart morphology, the end-diastolic and end-systolic RV areas (RVEDA and RVESA) along with the end-diastolic RV wall thickness (RVWTd) were measured using the left apical four-chamber view optimized for the right heart (RV focus view), as described previously (18–20). Each variable except for the RVWTd was measured by tracing the endocardial border of the right ventricle and normalized by body weight (20).

$$\text{RVEDA index} = \frac{(\text{RVEDA } [\text{cm}^2])}{(\text{body weight } [\text{kg}])^{0.624}}$$

$$\text{RVESA index} = \frac{\text{RVESA } (\text{cm}^2)}{\text{body weight } (\text{kg})^{0.628}}$$

The RVWTd was measured as the largest diameter of the RV free wall at end-diastole using the B-mode method. Additionally, the ratio of pulmonary artery to aortic diameter (PA:Ao) was obtained from the right parasternal short-axis view at the level of the pulmonary artery, as described previously (21).

Tricuspid annular plane systolic excursion (TAPSE), RV fractional area change, peak systolic change (RV FAC), tissue Doppler imaging-derived peak systolic myocardial velocity of lateral tricuspid annulus (RV s'), RV myocardial performance index (RV MPI), RV stroke volume (RV SV), and RV cardiac output (RV CO) were measured as indicators of RV systolic function, as described previously (19, 20, 22). All RV functional variables were obtained from the RV focus view. The TAPSE was measured using the B-mode method as described previously (23–25). The TAPSE and RV FAC were normalized by body weight using the following formula (22, 25):

$$\text{TAPSEn} = \frac{(\text{TAPSE } [\text{cm}])}{(\text{body weight } [\text{kg}])^{0.284}}$$

$$\text{RV FACn} = \frac{(\text{RV FAC } [\%])}{(\text{body weight } [\text{kg}])^{-0.097}}$$

The RV MPI was obtained from the tissue Doppler imaging-derived lateral tricuspid annular motion wave using the following formula:

$$\text{RV MPI} = \frac{(\text{b} - \text{a})}{\text{a}}$$

where a is the duration of the systolic tricuspid annular motion wave, and b is the interval from the end of the late diastolic tricuspid annular motion wave to the onset of the early diastolic tricuspid annular motion wave (19). The RV SV was calculated by multiplying the velocity-time integral of the pulmonary artery flow and the cross-sectional area of the pulmonary trunk obtained from the right parasternal short-axis view at the level of pulmonary artery, as described previously (26). The RV CO was obtained using RV SV and heart rate calculated by mean R-R intervals obtained from the same cardiac cycle used for RV SV measurement.

If the dogs had tricuspid valve or pulmonary valve regurgitation, we classified these severities as mild, moderate, or severe using color Doppler and continuous wave Doppler methods, as described previously (27, 28).

Two-Dimensional Speckle Tracking Echocardiography

All 2D-STE analyses were performed by a single investigator using the same ultrasound machine and evaluated by the same investigator using the same offline workstation as that used for standard echocardiography. The strain and strain

rate were obtained from the RV focus view using the left ventricular four-chamber algorithms (23, 29). The region of interest for 2D-STE was defined by manually tracing the RV endocardial border. Only RV free wall analysis (3seg) was performed by tracing from the level of the lateral tricuspid annulus to the RV apex for the longitudinal strain (RV-SL_{3seg}) and strain rate (RV-SrL_{3seg}) (**Figure 1A**). Right ventricular global analysis (6seg) was also performed by tracing from the lateral tricuspid annulus to the septal tricuspid annulus (including the interventricular septum) *via* the RV apex for the 6seg longitudinal strain (RV-SL_{6seg}), and strain rate (RV-SrL_{6seg}) (**Figure 1B**). Manual adjustments were made to include and track the entire myocardial thickness over the cardiac cycle when necessary. When the automated software could not track the myocardial regions, the regions of interest were retraced and recalculated. The RV-SL was defined as the absolute value of the negative peak value obtained from the strain wave (23, 30). The RV-SrL was obtained from the strain rate wave and was defined as the absolute value of the negative peak value during systole (30–32).

Variability of Intra- and Inter-Observer Measurements

Intra-observer measurement of variability was performed by a single observer who performed all the echocardiographic and radiographic measurements (YY). The baseline RV morphological and functional indices were obtained from the seven dogs. All measurements were performed on two different days at >7-day intervals using the same cardiogram and cardiac cycles. A second blinded observer (HK) measured the same indices for the determination of inter-observer variability using the same echocardiogram and heart cycles.

Statistical Analysis

All statistical analyses were performed using the commercially available EZR software, version 1.41 (Saitama Medical Center, Jichi Medical University, Saitama, Japan) (33). All continuous data were reported as median (interquartile range).

The normality of data was tested using the Shapiro–Wilk test. Continuous variables were compared between each timepoint by means of repeated measures analysis of variance with subsequent pairwise comparisons using the Bonferroni-adjusted paired *t*-test for normally distributed data or Friedman rank sum test with subsequent pairwise comparisons using the Bonferroni-adjusted Wilcoxon signed rank sum test for non-normally distributed data.

Variability of intra- and inter-observer measurements was quantified by the coefficient of variation (CV), which was calculated using the following formula:

$$\text{CV}\ (\%) = \frac{(\text{standard deviation})}{(\text{mean value})} \times 100$$

Intra- and inter-class correlation coefficients (ICC) were also used to evaluate the measurement variability. Low measurement variability was defined as CV < 10.0 and ICC > 0.7. Statistical significance was set at $P < 0.050$.

RESULTS

Creating PH Model Dogs

The dogs were administered repeated microsphere infusions for 2.2 ± 1.0, 6.9 ± 3.8, 14.9 ± 5.7, and 50.9 ± 13.1 weeks to meet the definition of sPAP30, sPAP40, sPAP50, and chronic, respectively. The median total dose of microspheres was 1.24 mg/kg (range: 0.93–1.37). There was no significant change in body weight. Two dogs required sedation with butorphanol tartrate and midazolam hydrochloride to perform echocardiography and for taking PAP measurements at each timepoint. None of the dogs showed any clinical symptoms associated with PH, including syncope, dyspnea, lethargy, ascites, and pleural effusion throughout this study protocol.

Hemodynamic Measurements

The hemodynamic data obtained from all seven model dogs were included in the statistical analysis. **Table 1** shows the results of hemodynamic parameters in the PH model dogs. With the rise in sPAP, the mean PAP also increased in the sPAP30, sPAP40, sPAP50, and chronic phases compared with the baseline ($P = 0.012$, $P = 0.018$, $P < 0.001$, and $P = 0.021$, respectively) parameters. The diastolic PAP was significantly increased in the sPAP50 and chronic phases compared with the baseline and sPAP30 values (sPAP50: $P = 0.003$ and $P = 0.004$, respectively; chronic: $P = 0.013$ and $P = 0.023$, respectively). There were no significant changes in systolic, mean, and diastolic systemic arterial pressure and heart rate with increased sPAP.

Echocardiographic Measurements

In this study, the echocardiographic data obtained from all seven model dogs were included in the statistical analysis. All the dogs had mild pulmonary valve regurgitation at baseline, sPAP30, and sPAP40 phases, and that was progressed to moderate at sPAP50 and chronic phases in four dogs (57%). Additionally, three dogs (43%) had mild tricuspid valve regurgitation at each timepoint.

Table 2 shows the results of echocardiographic parameters for RV morphology and function. The PA:Ao value was significantly higher in the sPAP50 phase than the baseline values and those of the sPAP40 phase ($P = 0.034$ and $P = 0.038$, respectively). This value was also significantly elevated in the chronic phase compared with those in the baseline, sPAP30, and sPAP40 phases ($P = 0.021$, $P = 0.004$, and $P = 0.010$, respectively). The RVEDA index and RVESA index were significantly increased in the chronic phase compared with those in the sPAP30 phase ($P = 0.041$ and $P = 0.048$, respectively). The RVWTd was significantly higher in the sPAP50 phase compared with that in baseline phase ($P = 0.042$). This value was also significantly elevated in the chronic phase compared with those in the baseline and sPAP30 phases ($P = 0.002$ and $P = 0.047$, respectively). The TAPSEn and RV MPI were significantly worse in the chronic phase compared with the baseline values ($P = 0.008$ and $P = 0.003$,

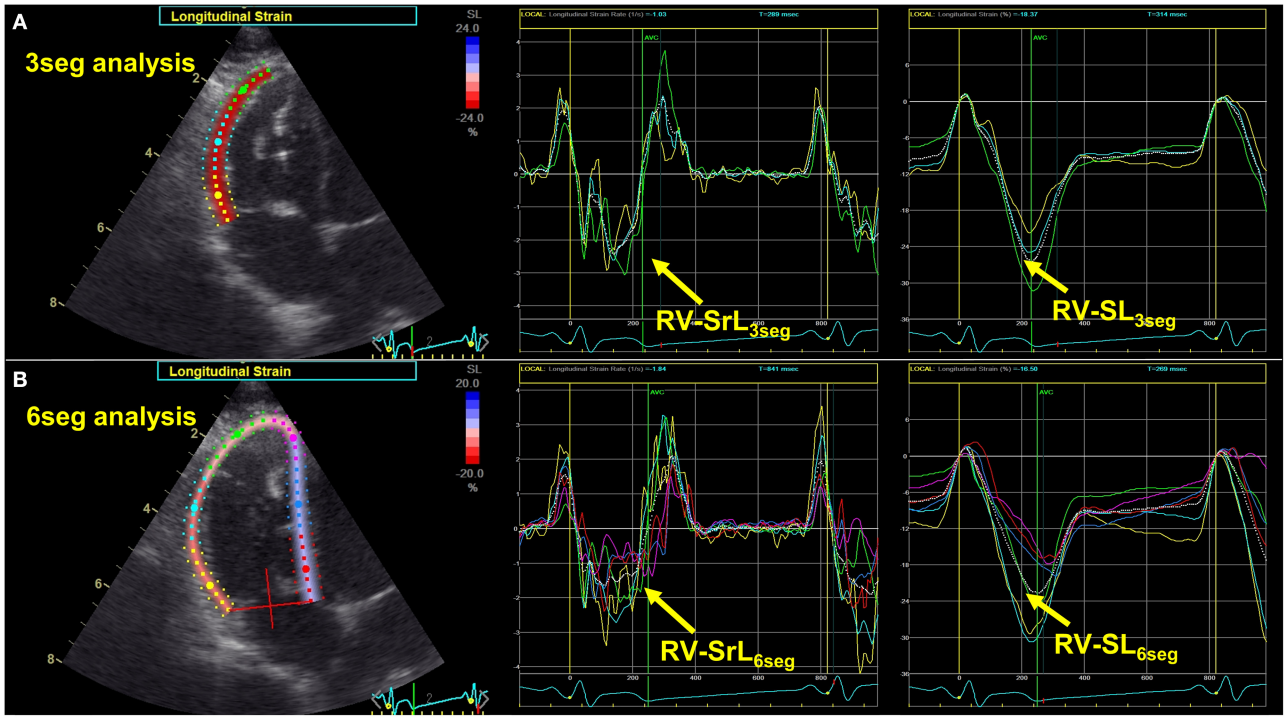

FIGURE 1 | Two-dimensional speckle tracking echocardiography-derived right ventricular longitudinal strain and strain rate (RV-SL and RV-SrL, respectively). **(A)** RV-SL and RV-SrL of the right ventricular free wall ($RV\text{-}SL_{3seg}$ and $RV\text{-}SrL_{3seg}$, respectively). **(B)** RV-SL and RV-SrL of the global right ventricle ($RV\text{-}SL_{6seg}$ and $RV\text{-}SrL_{6seg}$, respectively).

TABLE 1 | Changes in hemodynamic parameters during the process of creating canine models of chronic embolic pulmonary hypertension.

Variables	Baseline	sPAP30	sPAP40	sPAP50	Chronic
Pulmonary arterial pressure (mmHg)					
Systole	20.0 (17.3, 24.6)	33.0 (30.0, 34.6)[a]	42.3 (40.4, 47.8)[ab]	52.4 (50.7, 52.9)[abc]	51.4 (50.3, 65.9)[abc]
Mean	12.8 (11.0, 15.0)	16.8 (16, 20.4)[a]	21.7 (18.3, 23.9)[ab]	29.4 (27.9, 33.7)[abc]	30.1 (29.3, 31.9)[abc]
Diastole	6.4 (5.1, 9.0)	8.8 (8.3, 12.6)	11.8 (7, 17.2)	16.1 (15.4, 18.8)[ab]	16.3 (15.2, 19.4)[ab]
Systemic arterial pressure (mmHg)					
Systole	126 (116, 134)	124 (113, 137)	132 (116, 136)	130 (130, 131)	128 (120, 142)
Mean	92 (88, 97)	91 (78, 106)	97 (81, 107)	99 (91, 102)	93 (82, 98)
Diastole	80 (70, 82)	75 (65, 87)	82 (64, 93)	80 (73, 88)	69 (60, 77)
Heart rate (bpm)	88 (81, 115)	99 (91, 120)	102 (82, 124)	94 (64, 112)	84 (81, 100)

Continuous variables were displayed as median (interquartile range).
[a] *The value is significantly different from the Baseline ($P < 0.050$).*
[b] *The value is significantly different from the sPAP30 ($P < 0.050$).*
[c] *The value is significantly different from the sPAP40 ($P < 0.050$).*

respectively). The RV SV was significantly higher in the chronic phase compared with that in the sPAP30 phase ($P = 0.016$), whereas, RV FACn, RV s', and RV CO showed no significant changes with increased sPAP.

The results of 2D-STE indices are summarized in **Figures 2**, **3**. The $RV\text{-}SL_{3seg}$ and $RV\text{-}SL_{6seg}$ were significantly decreased in the sPAP30 phase compared with the baseline values ($P = 0.047$ and $P = 0.040$, respectively). Additionally, $RV\text{-}SL_{3seg}$ was significantly lower in the chronic phase compared with those in the baseline, sPAP40, and sPAP50 phases ($P = 0.012$, $P = 0.010$, and $P = 0.011$, respectively) (**Figure 2A**). However, $RV\text{-}SL_{6seg}$ was significantly reduced in the chronic phase compared with those in the baseline and sPAP40 phases ($P = 0.047$ and $P = 0.044$, respectively) (**Figure 2B**). The $RV\text{-}SrL_{3seg}$ and $RV\text{-}SrL_{6seg}$ were significantly lower in the chronic phase compared with those in the sPAP50 and sPAP40

TABLE 2 | Changes in echocardiographic parameters during the process of creating canine models of chronic embolic pulmonary hypertension.

Variables	Baseline	sPAP30	sPAP40	sPAP50	Chronic
PA:Ao	0.80 (0.78, 0.81)	0.78 (0.76, 0.81)	0.78 (0.74, 0.79)	0.92 (0.85, 0.93)[ac]	0.97 (0.96, 0.99)[abc]
RVEDA index ($cm^2/kg^{0.624}$)	1.43 (1.11, 1.44)	1.08 (0.91, 1.17)	1.02 (0.96, 1.27)	1.08 (0.96, 1.14)	1.47 (1.28, 1.63)[b]
RVESA index ($cm^2/kg^{0.628}$)	0.77 (0.60, 0.85)	0.73 (0.55, 0.82)	0.72 (0.52, 0.82)	0.65 (0.60, 0.72)	0.99 (0.88, 1.10)[b]
RVWTd (mm)	3.7 (3.4, 3.8)	4.0 (3.8, 4.2)	4.4 (3.9, 4.9)	4.9 (4.5, 5.0)[a]	5.6 (5.2, 6.1)[ab]
RV FACn (%/$kg^{-0.097}$)	53.7 (49.1, 61.0)	47.9 (46.3, 50.2)	44.0 (42.7, 56.6)	47.7 (41.6, 50.1)	37.1 (36.7, 40.0)
TAPSEn (mm/$kg^{0.33}$)	6.2 (5.9, 6.6)	5.5 (3.9, 5.9)	6.2 (6.0, 6.6)	5.9 (5.3, 6.4)	4.6 (4.3, 5.5)[a]
RV s' (cm/s)	11.0 (10.6, 12.2)	11.8 (9.8, 14.0)	13.1 (11.6, 14.8)	13.4 (11.6, 14.7)	9.1 (7.6, 11.0)
RV MPI	0.41 (0.36, 0.43)	0.41 (0.39, 0.56)	0.55 (0.43, 0.64)	0.55 (0.44, 0.62)	0.72 (0.68, 0.76)[a]
RV SV (mL)	18.5 (16.1, 19.4)	15.0 (10.9, 16.6)	15.5 (13.4, 17.6)	16.9 (15.7, 21.7)	21.8 (20.8, 23.4)[b]
RV CO (L/min)	1.5 (1.3, 2.2)	1.5 (1.4, 1.6)	1.5 (1.3, 1.9)	1.5 (1.4, 1.6)	1.8 (1.7, 2.1)

PA:Ao, pulmonary artery to aortic diameter ratio; RV CO, right ventricular cardiac output; RV FACn, right ventricular fractional area change normalized by body weight; RV MPI, right ventricular myocardial performance index; RV s', tissue Doppler imaging-derived peak systolic myocardial velocity of lateral tricuspid annulus; RV SV, right ventricular stroke volume; RVEDA index, end-diastolic right ventricular area normalized by body weight; RVESA index, end-systolic right ventricular area normalized by body weight; RVWTd, end-diastolic right ventricular wall thickness; TAPSEn, tricuspid annular plane systolic excursion normalized by body weight.

Continuous variables were displayed as median (interquartile range).

[a] The value is significantly different from Baseline ($P < 0.050$).

[b] The value is significantly different from sPAP30 ($P < 0.050$).

[c] The value is significantly different from sPAP40 ($P < 0.050$).

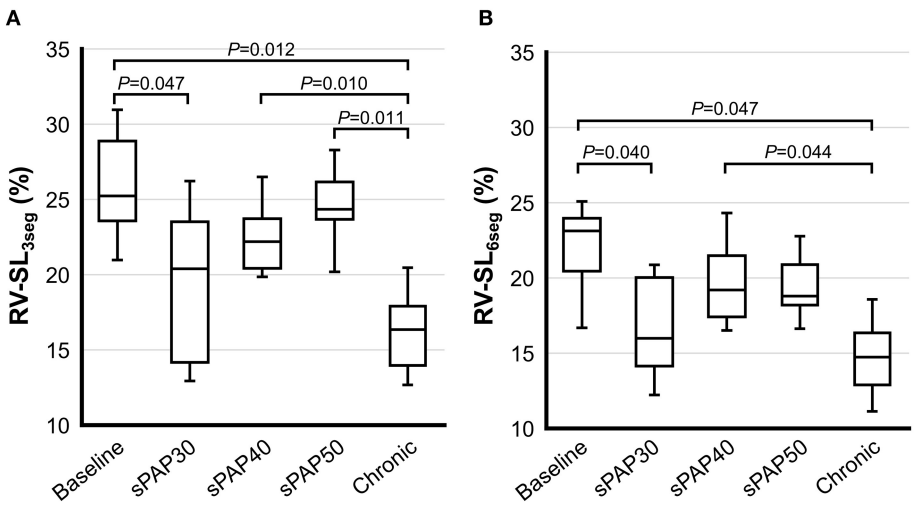

FIGURE 2 | Box and whisker plots of the right ventricular longitudinal strain (RV-SL) obtained from two-dimensional speckle tracking echocardiography. The bottom of the box is 25%, the middle line is the median, the top of the box is 75%, and the whiskers represent the range. **(A)** RV-SL of the right ventricular free wall ($RV\text{-}SL_{3seg}$). **(B)** RV-SL of the global right ventricle ($RV\text{-}SL_{6seg}$).

phases, respectively ($P = 0.028$ and $P = 0.039$, respectively) (**Figure 3**).

Intra- and Inter-Observer Measurement Variability

The results of intra- and inter-observer measurement variability for the echocardiographic indices assessed in this study are summarized in **Table 3**. Considering the intra-observer measurement variability, all the echocardiographic parameters showed low measurement variability. Further, all the echocardiographic indices except for RVESA, RV FAC, and RV MPI showed low measurement variability based on CV and ICC.

DISCUSSION

We created model dogs with chronic pre-capillary PH with moderately increased PAP and substantial right heart remodeling and compared the changes in RV function associated with increased PAP that was measured invasively in conscious dogs. In the acute phase, 2D-STE-derived RV systolic function was temporarily decreased due to the acute rise in PAP; however, it improved with RV hypertrophy; this may be a sign of RV adaptive remodeling. In contrast to the acute phase, RV systolic dysfunction assessed by RV-SL and RV dilatation were observed in the chronic phase of PH, which could be because of RV maladaptive remodeling and myocardial dysfunction.

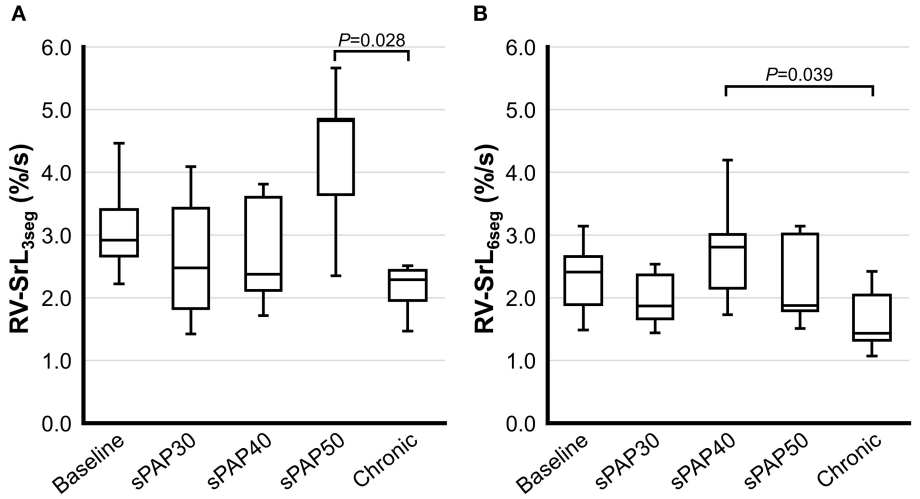

FIGURE 3 | Box and whisker plots of the right ventricular longitudinal strain rate (RV-SrL) obtained from two-dimensional speckle tracking echocardiography. The bottom of the box is 25%, the middle line is the median, the top of the box is 75%, and the whiskers represent the range. **(A)** RV-SrL of the right ventricular free wall ($RV\text{-}SrL_{3seg}$). **(B)** RV-SrL of the global right ventricle ($RV\text{-}SrL_{6seg}$).

TABLE 3 | Inter- and intra-observer measurement variability for echocardiographic parameters evaluated in this study.

Variables	Intra-observer			Inter-observer		
	CV (%)	ICC	*P*	CV (%)	ICC	*P*
PA:Ao	4.2	0.94	< 0.001	5.9	0.80	0.012
RVEDA	4.1	0.99	< 0.001	8.6	0.82	< 0.001
RVESA	5.8	0.94	< 0.001	11.4	0.66	0.012
RVWTd	3.2	0.93	< 0.001	6.5	0.80	0.004
RV FAC	5.0	0.81	0.001	8.8	0.50	0.002
TAPSE	3.1	0.90	< 0.001	5.9	0.80	0.002
RV s'	2.8	0.97	< 0.001	2.9	0.95	< 0.001
RV MPI	7.8	0.88	< 0.001	12.3	0.64	0.002
RV SV	4.4	0.98	< 0.001	8.9	0.94	< 0.001
$RV\text{-}SL_{3seg}$	4.4	0.93	< 0.001	5.0	0.92	< 0.001
$RV\text{-}SrL_{3seg}$	6.1	0.95	< 0.001	9.3	0.89	< 0.001
$RV\text{-}SL_{6seg}$	5.2	0.90	< 0.001	7.2	0.85	< 0.001
$RV\text{-}SrL_{6seg}$	5.8	0.94	< 0.001	7.6	0.93	< 0.001

3seg, only right ventricular free wall analysis; 6seg, right ventricular global analysis; CI, confidence interval; CV, coefficient of variation; ICC, intra- or inter-class correlation coefficients; PA:Ao, pulmonary artery to aortic diameter ratio; RV FAC, right ventricular fractional area change; RV MPI, right ventricular myocardial performance index; RV s', tissue Doppler imaging-derived peak systolic myocardial velocity of lateral tricuspid annulus; RV SV, right ventricular stroke volume; RVEDA, end-diastolic right ventricular area; RVESA, end-systolic right ventricular area; RV-SL, right ventricular longitudinal strain; RV-SrL, right ventricular longitudinal strain rate; RVWTd, end-diastolic right ventricular wall thickness; TAPSE, tricuspid annular plane systolic excursion.

In this study, certain conventional echocardiographic indices, such as TAPSEn and RV MPI, did not significantly change with increased PAP in the acute phase, although these indices were significantly worse in the chronic phase of PH. Nonetheless, 2D-STE indices showed substantial changes in the acute phase as well as in the chronic phase of PH. Previous studies reported that these conventional echocardiographic indices are affected by angle- and load-dependent limitations (34–36). Furthermore, all the model dogs in our study had echocardiographic evidence of tricuspid valve and pulmonary valve regurgitation; therefore, these volume overloads may prevent the detection of RV dysfunction using conventional indices. In contrast, 2D-STE variables have been used to assess intrinsic RV myocardial function with angle-independency and the low effect of these loading conditions (10). Additionally, considering PH would induce full RV remodeling against RV pressure overload, assessment of the global right ventricular function based on 2D-STE indices may help detect precise RV myocardial function more sensitively than conventional indices. Therefore, 2D-STE indices can be used to detect changes in intrinsic RV systolic function, which cannot be detected using conventional indices.

In the acute phase, RV-SL was significantly reduced in the sPAP30 phase and gradually increased in the sPAP40 and sPAP50 phases. In the sPAP30 phase, all the dogs did not have RV remodeling; therefore, the acute rise in PAP might have induced the imbalance between RV contractility and RV pressure overload (i.e., RV arterial uncoupling caused by increased RV pressure overload). However, RV-SL gradually increased with PAP and RVWTd, which indicates RV adaptive remodeling. In human medicine, RV adaptation remodeling was induced in PH patients through various mechanisms such as neurological activation, inflammation, and altered bioenergetics (19, 37, 38). In this study, the RVWTd gradually increased with the rise in PAP during the process of creating the chronic PH model dogs. Therefore, our results indicate that 2D-STE indices may be highly sensitive to changes that reflect the adaptation in RV myocardial contractility.

There was a significant difference between the 2D-STE-derived RV systolic functional indices of the sPAP50 and the chronic phases, although there was no significant difference in the RV loading condition (sPAP was stable at 50 mmHg). In general, chronic RV pressure overload increases myocardial wall stress, which in turn increases RV wall thickness and contractility to maintain RV CO (6–9). However, the RV myocardial contractility may be unable to cope with the chronic, excessive pressure overload. Our results suggest that RV-SL may reflect the intrinsic RV myocardial contractility, which showed decompensation in the chronic phase. Additionally, myocardial fibrosis might have also affected the results. Several studies have reported the prevalence of RV myocardial fibrosis in patients with PH (39, 40). Furthermore, in human patients with severe heart failure, the 2D-STE-derived RV-SL was reported to have a strong correlation with RV myocardial fibrosis, which could induce RV maladaptive remodeling and subsequent RV myocardial dysfunction (41). Although we have not conducted histopathological examinations in all the model dogs, the changes in RV-SL may also be indicative of RV fibrosis and RV maladaptation with PH progression.

In this study, RV-SL changed more drastically in 3seg than in 6seg in the acute phase, although both indices were significantly decreased in the chronic phase. Considering the interventricular septum when evaluating RV function is a matter of controversy (14, 42). A previous study has reported that RV-SL in the RV free wall is more sensitive to mild RV pressure overload than that in the interventricular septum (14). Our results also suggest that 2D-STE indices in the RV free wall may be more sensitive to increased RV pressure overload than those in the interventricular septum in dogs with moderate RV pressure overload. However, through the current 2D-STE assessment, we could not distinguish between the interventricular septum function of the RV and left ventricular components. Our results may vary in dogs with moderate PH secondary to left heart disease, which might impair the septal left ventricular function. Further studies to assess the precise myocardial function of both ventricles in dogs with PH secondary to left heart disease are expected in the future.

Our study has several limitations. First, the results were obtained from dogs with PH that was experimentally induced by microsphere infusion, which may vary in actual clinical settings or dogs with PH. Additionally, our findings may not be applicable in dogs with PH because of other causes such as left heart disease owing to its different pathophysiology that can increase PAP. Further studies are warranted to evaluate the relationship between echocardiographic indices and invasive PAP in dogs with spontaneous PH. Second, two of the seven dogs were sedated using butorphanol tartrate and midazolam hydrochloride. However, sedation with these agents have minimal effect on cardiovascular function (43). Furthermore, in dogs that required sedation so that hemodynamic measurements could be taken and echocardiography could be performed, these agents were used throughout the study protocol. Thus, sedation would have had minimal effect on our results. Finally, we have evaluated only longitudinal RV strain and strain rate. RV circumferential function would also contribute to RV systolic function in addition to the longitudinal function (30, 44, 45).

In conclusion, our study found that 2D-STE-derived RV-SL was significantly decreased in the sPAP30 phase compared with that in the baseline phase; it gradually increased in the sPAP40 and sPAP50 phases compared with that in the sPAP30 phase and decreased in the chronic phase compared with the baseline and sPAP50 phases. These results suggest that this non-invasive echocardiographic variable may reflect the RV compensative mechanism against PH pathophysiology, which could not be detected by conventional echocardiographic indices for RV function.

DATA AVAILABILITY STATEMENT

The raw data supporting the conclusions of this article will be made available by the authors, without undue reservation.

ETHICS STATEMENT

The animal study was reviewed and approved by Ethical committee for laboratory animal use of the Nippon Veterinary and Life Science University.

AUTHOR CONTRIBUTIONS

YY performed the concept/design, data analysis/interpretation, drafting article, and critical revision of article. RS performed the concept/design, data analysis/interpretation, critical revision of article, and approved the article. HK performed the data analysis as the second observer. TT, HM, and HK performed data interpretation, critically revised the manuscript, and approved the article. All authors contributed to the article and approved the submitted version.

FUNDING

This work was partially supported by Japan Society for the Promotion of Science (JSPS) KAKENHI Grant Number 20K15667.

ACKNOWLEDGMENTS

The authors would like to express their deepest appreciation to Kana Yanagisawa for their technical assistance. This work was conducted at the Laboratory of Veterinary Internal Medicine, School of Veterinary Science, Faculty of Veterinary Medicine, Nippon Veterinary and Life Science University in Tokyo, Japan. Additionally, we would like to thank Editage (www.editage.com) for English language editing.

REFERENCES

1. Reinero C, Visser LC, Kellihan HB, Masseau I, Rozanski E, Clercx C, et al. ACVIM consensus statement guidelines for the diagnosis, classification, treatment, and monitoring of pulmonary hypertension in dogs. *J Vet Intern Med.* (2020) 34:549–73. doi: 10.1111/jvim.15725
2. Johnson L, Boon J, Orton EC. Clinical characteristics of 53 dogs with Doppler-derived evidence of pulmonary hypertension: 1992–1996. *J Vet Intern Med.* (1999) 13:440–7. doi: 10.1111/j.1939-1676.1999.tb01461.x
3. Borgarelli M, Abbott J, Braz-Ruivo L, Chiavegato D, Crosara S, Lamb K, et al. Prevalence and prognostic importance of pulmonary hypertension in dogs with myxomatous mitral valve disease. *J Vet Intern Med.* (2015) 29:569–74. doi: 10.1111/jvim.12564
4. Jaffey JA, Wiggen K, Leach SB, Masseau I, Girens RE, Reinero CR. Pulmonary hypertension secondary to respiratory disease and/or hypoxia in dogs: clinical features, diagnostic testing and survival. *Vet J.* (2019) 251:105347. doi: 10.1016/j.tvjl.2019.105347
5. Haddad F, Doyle R, Murphy DJ, Hunt SA. Right ventricular function in cardiovascular disease, part II: pathophysiology, clinical importance, and management of right ventricular failure. *Circulation.* (2008) 117:1717–31. doi: 10.1161/CIRCULATIONAHA.107.653584
6. Llucià-Valldeperas A, de Man FS, Bogaard HJ. Adaptation and maladaptation of the right ventricle in pulmonary vascular diseases. *Clin Chest Med.* (2021) 42:179–94. doi: 10.1016/j.ccm.2020.11.010
7. Ryan JJ, Huston J, Kutty S, Hatton ND, Bowman L, Tian L, et al. Right ventricular adaptation and failure in pulmonary arterial hypertension. *Can J Cardiol.* (2015) 31:391–406. doi: 10.1016/j.cjca.2015.01.023
8. Vonk Noordegraaf A, Westerhof BE, Westerhof N. The relationship between the right ventricle and its load in pulmonary hypertension. *J Am Coll Cardiol.* (2017) 69:236–43. doi: 10.1016/j.jacc.2016.10.047
9. Wauthy P, Pagnamenta A, Vassalli F, Naeije R, Brimioulle S. Right ventricular adaptation to pulmonary hypertension: an interspecies comparison. *Am J Physiol Circ Physiol.* (2004) 286:H1441–7. doi: 10.1152/ajpheart.00640.2003
10. Amundsen BH, Helle-Valle T, Edvardsen T, Torp H, Crosby J, Lyseggen E, et al. Noninvasive myocardial strain measurement by speckle tracking echocardiography: validation against sonomicrometry and tagged magnetic resonance imaging. *J Am Coll Cardiol.* (2006) 47:789–93. doi: 10.1016/j.jacc.2005.10.040
11. Potter E, Marwick TH. Assessment of left ventricular function by echocardiography: the case for routinely adding global longitudinal strain to ejection fraction. *JACC Cardiovasc Imaging.* (2018) 11:260–74. doi: 10.1016/j.jcmg.2017.11.017
12. Jamal F, Bergerot C, Argaud L, Loufouat J, Ovize M. Longitudinal strain quantitates regional right ventricular contractile function. *Am J Physiol Circ Physiol.* (2003) 285:H2842–7. doi: 10.1152/ajpheart.00218.2003
13. Akabane R, Shimano S, Sakatani A, Ogawa M, Nagakawa M, Miyakawa H, et al. Relationship between right heart echocardiographic parameters and invasive pulmonary artery pressures in canine models of chronic embolic pulmonary hypertension. *J Vet Med Sci.* (2019) 81:1485–91. doi: 10.1292/jvms.19-0350
14. Morita T, Nakamura K, Osuga T, Yokoyama N, Morishita K, Sasaki N, et al. Changes in right ventricular function assessed by echocardiography in dog models of mild RV pressure overload. *Echocardiography.* (2017) 34:1040–9. doi: 10.1111/echo.13560
15. Grubb T, Sager J, Gaynor JS, Montgomery E, Parker JA, Shafford H, et al. 2020 AAHA anesthesia and monitoring guidelines for dogs and cats. *J Am Anim Hosp Assoc.* (2020) 56:59–82. doi: 10.5326/JAAHA-MS-7055
16. Rothman A, Wiencek RG, Davidson S, Evans WN, Restrepo H, Sarukhanov V, et al. Challenges in the development of chronic pulmonary hypertension models in large animals. *Pulm Circ.* (2017) 7:156–66. doi: 10.1086/690099
17. Hori Y, Uchide T, Saitoh R, Thoei D, Uchida M, Yoshioka K, et al. Diagnostic utility of NT-proBNP and ANP in a canine model of chronic embolic pulmonary hypertension. *Vet J.* (2012) 194:215–21. doi: 10.1016/j.tvjl.2012.03.022
18. Visser LC, Scansen BA, Schober KE, Bonagura JD. Echocardiographic assessment of right ventricular systolic function in conscious healthy dogs: repeatability and reference intervals. *J Vet Cardiol.* (2015) 17:83–96. doi: 10.1016/j.jvc.2014.10.003
19. Rudski LG, Lai WW, Afilalo J, Hua L, Handschumacher MD, Chandrasekaran K, et al. Guidelines for the echocardiographic assessment of the right heart in adults: a report from the American Society of Echocardiography. Endorsed by the European Association of Echocardiography, a registered branch of the European Society of Cardiology, and the Canadian Society of Echocardiography. *J Am Soc Echocardiogr.* (2010) 23:685–713. doi: 10.1016/j.echo.2010.05.010
20. Gentile-Solomon JM, Abbott JA. Conventional echocardiographic assessment of the canine right heart: reference intervals and repeatability. *J Vet Cardiol.* (2016) 18:234–47. doi: 10.1016/j.jvc.2016.05.002
21. Visser LC, Im MK, Johnson LR, Stern JA. Diagnostic value of right pulmonary artery distensibility index in dogs with pulmonary hypertension: comparison with doppler echocardiographic estimates of pulmonary arterial pressure. *J Vet Intern Med.* (2016) 30:543–52. doi: 10.1111/jvim.13911
22. Visser LC, Scansen BA, Brown NV, Schober KE, Bonagura JD. Echocardiographic assessment of right ventricular systolic function in conscious healthy dogs following a single dose of pimobendan versus atenolol. *J Vet Cardiol.* (2015) 17:161–72. doi: 10.1016/j.jvc.2015.04.001
23. Yuchi Y, Suzuki R, Teshima T, Matsumoto H, Koyama H. Utility of tricuspid annular plane systolic excursion normalized by right ventricular size indices in dogs with postcapillary pulmonary hypertension. *J Vet Intern Med.* (2021) 35:107–19. doi: 10.1111/jvim.15984
24. Caivano D, Dickson D, Pariaut R, Stillman M, Rishniw M. Tricuspid annular plane systolic excursion-to-aortic ratio provides a bodyweight-independent measure of right ventricular systolic function in dogs. *J Vet Cardiol.* (2018) 20:79–91. doi: 10.1016/j.jvc.2018.01.005
25. Visser LC, Sintov DJ, Oldach MS. Evaluation of tricuspid annular plane systolic excursion measured by two-dimensional echocardiography in healthy dogs: repeatability, reference intervals, and comparison with M-mode assessment. *J Vet Cardiol.* (2018) 20:165–74. doi: 10.1016/j.jvc.2018.04.002
26. Lewis JF, Kuo LC, Nelson JG, Limacher MC, Quinones MA. Pulsed Doppler echocardiographic determination of stroke volume and cardiac output: clinical validation of two new methods using the apical window. *Circulation.* (1984) 70:425–31. doi: 10.1161/01.CIR.70.3.425
27. Lancellotti P, Moura L, Pierard LA, Agricola E, Popescu BA, Tribouilloy C, et al. European association of echocardiography recommendations for the assessment of valvular regurgitation. Part 2: mitral and tricuspid regurgitation (native valve disease). *Eur J Echocardiogr.* (2010) 11:307–32. doi: 10.1093/ejechocard/jeq031
28. Vezzosi T, Domenech O, Costa G, Marchesotti F, Venco L, Zini E, et al. Echocardiographic evaluation of the right ventricular dimension and systolic function in dogs with pulmonary hypertension. *J Vet Intern Med.* (2018) 32:1541–8. doi: 10.1111/jvim.15253
29. Suzuki R, Matsumoto H, Teshima T, Koyama H. Clinical assessment of systolic myocardial deformations in dogs with chronic mitral valve insufficiency using two-dimensional speckle-tracking echocardiography. *J Vet Cardiol.* (2013) 15:41–9. doi: 10.1016/j.jvc.2012.09.001

30. Suzuki R, Yuchi Y, Kanno H, Teshima T, Matsumoto H, Koyama H. Left and right myocardial functionality assessed by two-dimensional speckle-tracking echocardiography in cats with restrictive cardiomyopathy. *Animals.* (2021) 11:1578. doi: 10.3390/ani11061578
31. Suzuki R, Matsumoto H, Teshima T, Koyama H. Effect of age on myocardial function assessed by two-dimensional speckle-tracking echocardiography in healthy beagle dogs. *J Vet Cardiol.* (2013) 15:243–52. doi: 10.1016/j.jvc.2013.07.001
32. Suzuki R, Matsumoto H, Teshima T, Koyama H. Influence of heart rate on myocardial function using two-dimensional speckle-tracking echocardiography in healthy dogs. *J Vet Cardiol.* (2013) 15:139–46. doi: 10.1016/j.jvc.2012.12.004
33. Kanda Y. Investigation of the freely available easy-to-use software "EZR" for medical statistics. *Bone Marrow Transplant.* (2013) 48:452–8. doi: 10.1038/bmt.2012.244
34. Hsiao S-H, Lin S-K, Wang W-C, Yang S-H, Gin P-L, Liu C-P. Severe tricuspid regurgitation shows significant impact in the relationship among peak systolic tricuspid annular velocity, tricuspid annular plane systolic excursion, and right ventricular ejection fraction. *J Am Soc Echocardiogr.* (2006) 19:902–10. doi: 10.1016/j.echo.2006.01.014
35. Tidholm A, Höglund K, Häggström J, Ljungvall I. Diagnostic value of selected echocardiographic variables to identify pulmonary hypertension in dogs with myxomatous mitral valve disease. *J Vet Intern Med.* (2015) 29:1510–7. doi: 10.1111/jvim.13609
36. Morita T, Nakamura K, Osuga T, Yokoyama N, Morishita K, Sasaki N, et al. Effect of acute volume overload on echocardiographic indices of right ventricular function and dyssynchrony assessed by use of speckle tracking echocardiography in healthy dogs. *Am J Vet Res.* (2019) 80:51–60. doi: 10.2460/ajvr.80.1.51
37. Champion HC, Michelakis ED, Hassoun PM. Comprehensive invasive and non-invasive approach to the right ventricle-pulmonary circulation unit state of the art and clinical and research implications. *Circulation.* (2009) 120:992–1007. doi: 10.1161/CIRCULATIONAHA.106.674028
38. Benza RL, Miller DP, Gomberg-Maitland M, Frantz RP, Foreman AJ, Coffey CS, et al. Predicting survival in pulmonary arterial hypertension: insights from the registry to evaluate early and long-term pulmonary arterial hypertension disease management (REVEAL). *Circulation.* (2010) 122:164–72. doi: 10.1161/CIRCULATIONAHA.109.898122
39. Rain S, Handoko ML, Trip P, Gan CTJ, Westerhof N, Stienen GJ, et al. Right ventricular diastolic impairment in patients with pulmonary arterial hypertension. *Circulation.* (2013) 128:2016–25. doi: 10.1161/CIRCULATIONAHA.113.001873
40. Bogaard HJ, Natarajan R, Henderson SC, Long CS, Kraskauskas D, Smithson L, et al. Chronic pulmonary artery pressure elevation is insufficient to explain right heart failure. *Circulation.* (2009) 120:1951–60. doi: 10.1161/CIRCULATIONAHA.109.883843
41. Lisi M, Cameli M, Righini FM, Malandrino A, Tacchini D, Focardi M, et al. RV longitudinal deformation correlates with myocardial fibrosis in patients with end-stage heart failure. *JACC Cardiovasc Imaging.* (2015) 8:514–22. doi: 10.1016/j.jcmg.2014.12.026
42. Chetboul V, Damoiseaux C, Lefebvre HP, Concordet D, Desquilbet L, Gouni V, et al. Quantitative assessment of systolic and diastolic right ventricular function by echocardiography and speckle-tracking imaging: a prospective study in 104 dogs. *J Vet Sci.* (2018) 19:683–92. doi: 10.4142/jvs.2018.19.5.683
43. Kojima K, Nishimura R, Mutoh T, Takao K, Matsunaga S, Mochizuki M, et al. Comparison of cardiopulmonary effects of medetomidine-midazolam, acepromazine-butorphanol and midazolam-butorphanol in dogs. *J Vet Med Ser A Physiol Pathol Clin Med.* (1999) 46:353–9. doi: 10.1046/j.1439-0442.1999.00224.x
44. Vitarelli A, Terzano C. Do we have two hearts? New insights in right ventricular function supported by myocardial imaging echocardiography. *Hear Fail Rev.* (2010) 15:39–61. doi: 10.1007/s10741-009-9154-x
45. Caivano D, Rishniw M, Birettoni F, Petrescu VF, Porciello F. Transverse right ventricle strain and strain rate assessed by 2-dimensional speckle tracking echocardiography in dogs with pulmonary hypertension. *Vet Sci.* (2020) 7:1–10. doi: 10.3390/vetsci7010019

Conflict of Interest: HK received a grant from Toray Industries, Inc.

The remaining authors declare that the research was conducted in the absence of any commercial or financial relationships that could be construed as a potential conflict of interest.